Pergamon

0301-9322(93)E0012-T

Int. J. Multiphase Flow Vol. 20, No. 2, pp. 415–437, 1994

0301-9322/94 $7.00 + 0.00

ANALYSIS OF THE WET PRESSING OF PAPER PULP

J. LEWALLE,[1] K. M. SINGH[2]† and J. P. BAMBACHT[2]

[1]Department of Mechanical and Aerospace Engineering, Syracuse University, Syracuse, NY 13244, U.S.A.

[2]Paper Science and Engineering, SUNY—Environmental Science and Forestry, Syracuse, NY 13244, U.S.A.

(Received 23 January 1991; in revised form 19 October 1993)

Abstract—The equations governing the motion of the paper sheet in a press nip and the anisotropic percolation of the water in the sheet, are derived in invariant form. In order to avoid restrictive assumptions on the configuration of the paper sheet, the system of coordinates is generated by the flow of fibrous material through the nip region. With the corresponding constitutive equations, the formulation consists of a system of partial differential equations for the metric tensor of the coordinate system, and for the water velocity. For practical use, the solution is then mapped back into a cartesian frame of reference. Quantities of industrial interest, such as the residual water content and stresses, as well as the press-induced anisotropy, can be calculated in principle. A Galerkin finite-element approximation is implemented using rectangular linear elements. Two case studies are presented, for large and small permeabilities, and the corresponding differences in water pressure and velocity are in general qualitative agreement with the observations. Finally, the predictive value of the model is demonstrated by the dependence of the solution on the imposed shear stress and its gradient across the sheet.

Key Words: wet pressing, paper pulp, deforming porous media, percolation

1. INTRODUCTION

Few problems in the mechanics of porous media involve fast finite deformations of the solid phase in such a way that a Eulerian description of the flow field and the use of convective derivatives are required. The wet pressing of paper pulp is such a problem.

The wet pressing is carried out by squeezing the pulp on a felt mat by running it continuously between two hard rolls. In the process, some of the water is forced from the pulp into the felt, and some is forced out of the system. Research has been conducted in both the analytical and experimental areas. The theoretical approach consists of modeling the pressing process, and solving the corresponding equations of the fluid and solid motions. Some simplifying assumptions are made in the derivation of the model. In the experimental approach, emphasis is placed on the laboratory scale duplication of the actual process. Here too, the difficulty of performing the necessary measurements leaves us with an incomplete description of the process.

The earliest effort to model the wet pressing process was made by Campbell (1947). He assumed that the compression of the pulp is homogeneous and that all the pressure is borne by the fluid phase, both assumptions now known to be approximate at best. Starting from the Kozeny–Carmen equation for flow through porous media, he derived an equation to predict the time required to press a sheet of wet paper from one solid concentration to another. Campbell realized that the multiplication of pressing time and pressure, termed the pressing impulse by Wahlstrom (1960), is related to the change in consistency during pressing. Campbell's model accounted for the effect of the specific area of the pulp. As the water is pressed out of the pulp, the specific area increases. This increases the pressing impulse needed to cause a given increase in the solids content of the pulp being pressed. The importance of "impulse" is now well-established. Bullerwell & Baade's (1984) results show that the impulse is an effective way of characterizing a press, although the theory fails at extreme values of time or pressure.

†Present address: International Paper, Paper Science and Technology Department, Long Meadow Road, Tuxedo, NY 10987, U.S.A.

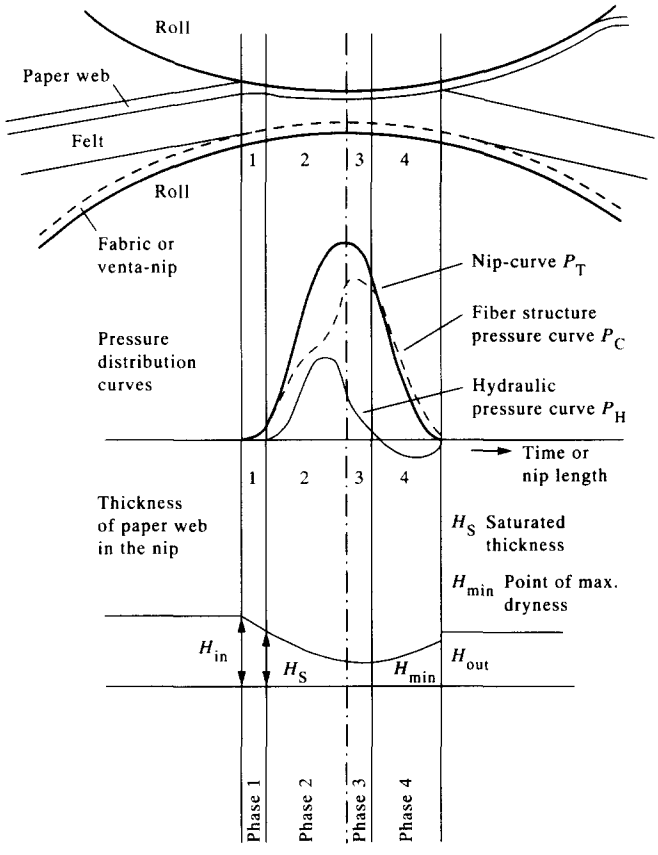

Figure 1. The 4 phases of the press nip, after Wahlstrom (1960).

The next advance in wet press modeling is due to Wahlstrom (1960). He divided the plain press nip into three phases, based mostly on geometrical considerations. Starting from a known geometry of a nip and using Darcy's law he concluded that water is removed from the paper into the felt in the first phase and then removed to the inlet side of the nip. In the second phase, he concluded that "rewetting" is taking place by capillary action. He also found the hydraulic pressure in a plain press to be much higher than in a suction press.

Nilsson & Larsson's (1964) model of the press nip divided it into four phases, as depicted on figure 1. The first phase extends from the entrance of the nip until the point where the sheet gets saturated. The second phase extends up to the middle of the nip; most water removal takes place in this phase. The third phase extends to the point where the hydraulic pressure becomes zero. The fourth phase consists of the rest of the residence time in the nip; in this phase, the felt and the sheet expand, and some rewetting of the paper sheet takes place. The amount of rewetting is still a matter of conjecture.

Wilder (1967) extended the overall material and force balances of the press nip, as presented by Wahlstrom (1960) and by Yih & McNamara (1964). He introduced the inertial term in Darcy's flow equation, which would be significant for higher flow velocities. In all these models, only velocities in a direction normal to the face of the paper sheet are considered.

In recent years, Carlsson *et al.* (1983) have modeled the paper behavior in the nip as that of a simple Kelvin element. Again, their attempt has been to model the overall pressure and downward flow velocity profiles. Their results indicate that the point of maximum hydraulic pressure need not be before the middle of the nip, as was predicted by Wahlstrom (1960).

Jewett (1980) approximated the paper mat as a homogeneous porous medium, with different points in the system being at different compression levels and hence at different pressure levels. The force and material balances and Darcy's law provided the basic equations, which were solved using the finite-difference technique. The presence and flow of air was accounted for. However, it is a one-dimensional model and more closely approximates the laboratory-scale flat-platen presses

than industrial continuous flow presses. The application of the model to industrial presses required the determination of an arbitrary scaling factor, termed the "nip efficiency".

MacGregor (1985) has presented some nonmathematical models based on his perception about what is going on in the nip. These are based on experimental work done by himself and by Beck (1983). In these models, the in-plane fluid velocity plays an important role in altering the structure of the paper.

Experimental work has mostly been done on flat-platen presses with various pulp types, surface configurations, pressure profiles and various ways of sensing the interfacial pressures and the change in thickness. Swain (1980) has studied the compressibility of various types of felts in a flat-platen press. Chang (1978) and Ceckler & Thompson (1982) have done exhaustive studies on the compressibility of paper mats in such apparatus. Ceckler & Thompson have attempted to apply the compressibility and permeability measurements to industrial presses, using Jewett's model. Some typical results are shown in figure 2. Carlsson *et al.* (1983) have also worked on similar apparatus and found that the "water retention value" of the pulp has a strong effect on the removal of the water. This implies that water is squeezed out of the fibers, in addition to the removal of the free water outside the fibers.

Beck (1983) studied the surface pressure profiles in an industrial scale press. His work indicated that the hydraulic pressure on the surface of a felt in a nip falls in a relatively wide range of values. It was also found that there are sharp pressure gradients over grooves or holes in "transversal flow" press rolls. This explains to some extent the shadow marking and groove marking in paper.

The purpose of this article is to establish a rigorous mathematical framework for the study of the pressure, stress and velocity fields, as well as the ultimate mechanical properties of the paper. Insofar as this article constitutes a first step in that direction, the emphasis is placed on generality and formalism, rather than on the realistic character of the system. Two significant elements in the problem were thus deleted temporarily. The role of the trapped air, and even the felt mat, are not described herein. How they can be accommodated in the model, is discussed in section 7. Such drastic simplifications are counterbalanced by a high level of generality in all other aspects of the analysis. All significant parameters identified previously are part of the model, or can be calculated from numerical results. A complete map of the mat configuration (bending), stresses, pressure and velocity fields, can be obtained under a variety of imposed boundary conditions. Such generality comes at the cost of more sophisticated techniques: tensor analysis in general coordinates turns out to be the right tool in this instance. The first part of the article is devoted to the derivation of the equations. The constitutive relations correspond to the simplest case of

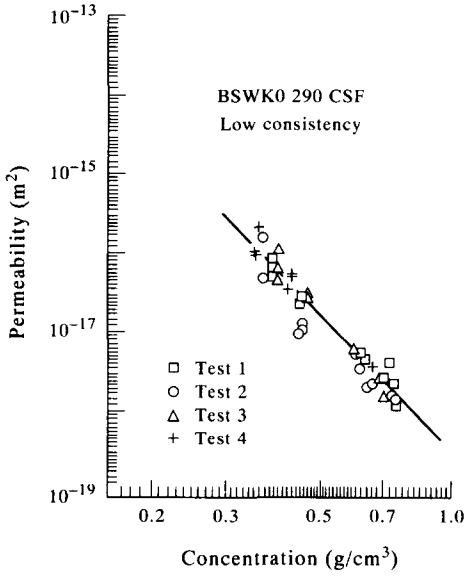

Figure 2. Permeability (m^2) vs concentration (g/cm^3), after Ceckler & Thompson (1982).

practical interest. The issue of the reference metric tensor and the mapping of streamlines is discussed next. Finally, the boundary conditions are derived.

2. FORMULATION OF THE PROBLEM—GENERAL EQUATIONS OF MOTION

Our approach starts from the observation that, when the motion of the fiber mat is described in cartesian coordinates, enormous difficulties are encountered in imposing realistic boundary conditions. The core of the issue is the actual location of the boundaries. Rather than assuming an approximate mat configuration, we decided to express the fact that the flow itself generates the boundary.

The coordinate system results from our choice to describe the wet pressing process in a Eulerian frame of reference. Then, the flow of material can be considered to be in steady-state. When we imagine material points flowing through a region of interest, the pathlines (identical to streaklines and to streamlines in a steady-state flow) identify one family of coordinates, including the boundary at the face of the sheet. The other family is identified as timelines, in which material lines (not parallel to the direction of the flow), released at some initial time, are mapped at regular intervals (see figure 3).

The system of coordinates is entirely determined if we fix the time interval and the initial (upstream) spacing of the pathlines. The choice will be made below, so as to simplify the relation between anisotropy and strain.

In this coordinate system, generated by the solid material, but not tied to it, the motion of the fiber mat will be similar to that of a fluid, except for the stress–strain constitutive relation. Thus, it is convenient to assume that the fiber mat can be described as a continuum. This assumption is not incompatible with the practical situation of a thin sheet, in which the thickness of the individual fibers is smaller than, but comparable to the sheet. Although the texture of the fibers is significant locally, the steady-state Eulerian description averages the fiber content over a period of time, in effect blurring the texture to a continuum. This is the same assumption made by a number of authors in the study of mixtures [e.g. Green & Naghdi (1965, 1979), Thigpen & Berryman (1985), Bedford & Drumheller (1983) and Allen (1985) among others; see also Eringen (1976) for a thorough presentation], allowing for the construction of constitutive relations satisfying the axioms of rational mechanics.

The coordinate system in which both fiber and water flows will be described is obviously not rectangular; moreover, the local base vectors, determined by the spacing between coordinate surfaces, are not normalized. Thus, the partial differential equations of motion must be written in tensor notation, with co- and contravariance denoted by sub- and superscripts, respectively. All derivatives in the general theory, must be understood to be with the correct variance. Thus, notational changes are made to the paper of Thigpen & Berryman (1985), where the assumption

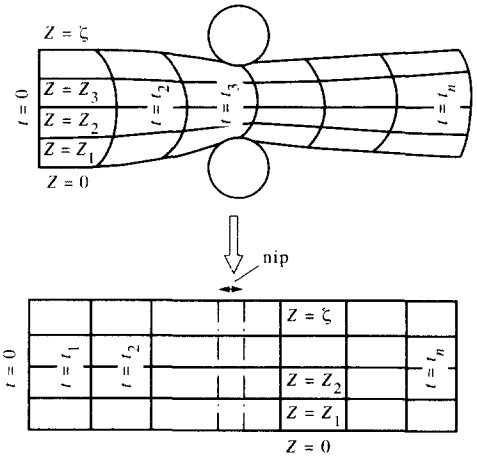

Figure 3. Generation of the coordinate system as streamlines and timelines of the fiber motion.

of an elastic solid phase corresponds to our needs. However, their assumption of small solid velocities is inadequate in our case, and changes are made accordingly.

In the derivation of the general equations, the metric tensor does not have to be specified, other than to use the fact that it is generated by the fiber flow. The effect of the specific choice of the coordinate system on the metric tensor and the velocity vectors, will be discussed below.

In succession, we will address the mass conservation (continuity) equations for the water and the solid, and the respective momentum equations. The velocity vectors will be denoted as $\mathbf{v}$ for for the water and $\mathbf{u}$ for the fiber mat.

Water can be considered as an incompressible fluid for most applications. The incompressibility condition is expressed by the kinematic constraint that $\operatorname{div} \mathbf{v} = 0$. However, in curvilinear coordinates, the expression for the divergence must reflect the fact that the base vectors themselves change from point to point. The general expression is thus

$$\frac{\mathrm{D}v^k}{\mathrm{D}x^k} = \frac{\partial v^k}{\partial x^k} + v^i \Gamma^k_{k\,i} = 0 \qquad [1]$$

and

$$\Gamma^j_{ik} = \frac{1}{2} g^{jm}\left(\frac{\partial}{\partial x^i} g_{km} + \frac{\partial}{\partial x^k} g_{im} - \frac{\partial}{\partial x^m} g_{ik}\right) = \Gamma^j_{k\,i}; \qquad [2]$$

Γ^j_{ik} is the Christoffel symbol of second kind. The Γ term accounts for the change in metric from point to point e.g. Flügge (1972).

The solid material experiences deformations as it flows from one location to the next. In the process, some of the water permeating the fibers is forced out, the volume occupied by a given set of fibers decreases and shear deformations take place as well. However, as the fiber flow generates the coordinate surfaces, the conservation of mass should be expressed as *apparent* incompressibility. In other words, the fiber mat is compressible in fact, but any change in specific volume is accounted for by the change in metric of the coordinate system. Thus,

$$\frac{\partial u^k}{\partial x^k} = 0.\dagger \qquad [3]$$

The momentum equations are written next. Under our assumption that the solid and the liquid phases are overlapping immiscible continua, the fundamental equations of rational mechanics apply. Because temperature is assumed to be uniform in the web, and among the phases, no energy considerations need be introduced. As a further simplification from the general theory of mixtures, we assume that mass diffusion is not dynamically significant, based on the lack of evidence to the contrary.

In steady-state motion, the convective derivative of the velocity field is to balance the applied and internal forces per unit mass. The familiar flow equations can be used, provided we use covariant derivatives. Thus,

$$\rho v^j \frac{\mathrm{D}v^i}{\mathrm{D}x^j} = f^i + \frac{\mathrm{D}\tau^{ij}}{\mathrm{D}x^j} \qquad [6]$$

and

$$Pu^j \frac{\mathrm{D}u^i}{\mathrm{D}x^j} = F^i + \frac{\mathrm{D}T^{ij}}{\mathrm{D}x^j}, \qquad [7]$$

---

†Consistency with this result is observed if mass conservation is derived in detail. The fiber density is inversely proportional to the square root of the determinant of the metric tensor:

$$g = \mathrm{dtm}\, g_{ij}. \qquad [4]$$

Then the mass conservation equation is expressed in invariant form as

$$\frac{\mathrm{D}}{\mathrm{D}x^k}\frac{u^k}{\sqrt{g}} = \frac{1}{\sqrt{g}}\left(\frac{\partial u^k}{\partial x^k} + u^i \Gamma^k_{k\,i}\right) - \frac{u^k}{\sqrt{g}} \Gamma^i_{k\,i} = 0, \qquad [5]$$

equivalent to [3].

where ρ and P are the densities of the water and the solid, respectively. The right-hand-side terms contain the interphase forces and the single-phase stresses in the water and the solid. These equations are a particular case of those used by Thigpen & Berryman (1985), where we neglect body forces and gradients in the phase fraction of solid and water. All displacements in the solid must also satisfy the compatibility equation, more easily spelled out below, [15].

3. CONSTITUTIVE RELATIONS

The rational theories mentioned in the previous section provide the framework for the general form of the constitutive relations, which enable us to express the forces and stresses in terms of the primary dependent variables (v and u). Again, we shall use the results of Thigpen & Berryman (1985), which include the case of a gaseous phase as well, with simplifications that appear reasonable for a first study of the wet pressing process.

The stress tensors must be given by constitutive equations, expressing the response of the materials to imposed conditions. In this context, where the possibilities of the model are being explored, the balance between generality and simplicity is difficult to gauge. Simplicity cannot be at the expense of a realistic character of the process: to that extent, the fact that the theory of Thigpen & Berryman (1985) includes the motion of air opens the way for eventual generalizations. More importantly, once the simplified problem (saturated mat) has been identified, the thermodynamic constraints and the invariance properties derived from the rational mechanics of constitutive equations may not be violated.

Thus, it is sensible and consistent with our approach to take the equations of Thigpen & Berryman (1985), with certain terms deleted if they are thought to be unimportant in wet pressing, as long as the theory is not violated. Other changes to the theory are required by the fact that the velocity of the solid phase is large, and that displacements from a reference location are not suitable in a Eulerian description.

The construction of invariant constitutive relations depends on the list of admissible primary variables. For the fluid, the stress would depend on the local metric, and on the symmetric part of the (covariant) velocity gradients, by analogy with the classical theory. Thus, in the absence of physical indications to the contrary, the list of primary variables is closed, and the constitutive relation must be of the form

$$\tau^{ij}(g^{ij}, s^{ij}), \tag{8}$$

where

$$s^{ij} = \frac{1}{2}\left(g^{jk}\frac{\mathrm{D}v^i}{\mathrm{D}x^k} + g^{ik}\frac{\mathrm{D}v^j}{\mathrm{D}x^k}\right). \tag{9}$$

Within this class of constitutive equations, the dependence will be limited to linear expressions in the arguments. In continuum mechanics, this is known to be a rational approximation, satisfactory in many engineering problems. Then,

$$\tau^{ij} = -\pi g^{ij} + 2\mu s^{ij}. \tag{10}$$

In [10], π and μ are functions of the scalar invariants of g and s, to be determined either experimentally or for most effective simplification of the equations. Within the framework of Navier–Stokes fluids, π can be interpreted as pressure, and will vary from point to point: it will provide the connection to the equations for the solid below. In line with our strategy to simplify equations as much as possible, the other parameters, such as μ, will be considered as independent of any flow quantity.

For an elastic solid (see appendix A for a viscoelastic case), the constitutive relation is even simpler, since the strain tensor is equal to the departure of the local metric tensor from its initial value. From an elastic material, we have the stress–strain relation

$$T^{ij}(\gamma_{ij}),$$

where

$$\gamma_{ij} = g_{ij} - g^0_{ij}.$$

The linear approximation to the functional dependence (e.g. Flügge 1972) gives

$$T^{ij} = \frac{E^{ijkm}\gamma_{km}}{2}, \qquad [11]$$

where

$$E^{ijkm} = \frac{E}{2(1+\nu)}\left(\frac{2\nu}{1-2\nu}g^{ij}g^{km} + g^{ik}g^{jm} + g^{im}g^{jk}\right) \qquad [12]$$

for the elastic case. Here, E is Hooke's modulus and ν is the Poisson coefficient. For later convenience, the stress tensor can be split into its isotropic and deviatoric parts. We find

$$T^{ij} = g^{ij}\frac{E}{6(1+\nu)}g^{km}\gamma_{km} + \frac{E}{2(1+\nu)}(-g^{ij}g^{km} + \tfrac{1}{2}g^{ik}g^{jm} + \tfrac{1}{2}g^{im}g^{jk})\gamma_{km}. \qquad [13]$$

Hence, the force term in the momentum equation can be calculated, when we remember that the covariant derivative of the metric tensor vanishes identically and that the covariant derivative of a scalar reduces to its partial derivative:

$$\frac{\mathrm{D}T^{ij}}{\mathrm{D}x^j} = -g^{ij}\frac{\partial \Pi}{\partial x^j} + \frac{E}{2(1+\nu)}\frac{\mathrm{D}}{\mathrm{D}x^j}(-g^{ij}g^{km} + \tfrac{1}{2}g^{ik}g^{jm} + \tfrac{1}{2}g^{im}g^{jk})\gamma_{km}, \qquad [14]$$

where

$$\Pi = -\frac{E}{6(1+\nu)}g^{km}\gamma_{km}.$$

Finally, the displacements in the solid must satisfy the compatibility equation

$$\frac{\mathrm{D}^2\gamma_{11}}{\mathrm{D}x_2^2} + \frac{\mathrm{D}^2\gamma_{22}}{\mathrm{D}x_1^2} - 2\frac{\mathrm{D}^2\gamma_{12}}{\mathrm{D}x_1\mathrm{D}x_2} = 0. \qquad [15]$$

4. INTERPHASE FORCES AND CHOICE OF THE INITIAL METRIC

The interphase forces can be constructed in a similar manner (Bedford & Drumheller 1983). Since gravity is not expected to be relevant to the flow dynamics, the list of variables can be limited to the difference in velocity between the phases, and possibly the metric or deformation tensor. The only invariant form resulting from this list is, in the linear approximation, the Darcy term

$$f^i = \alpha(u^i - v^i) \qquad [16]$$

and

$$F^i = \beta(u^i - v^i), \qquad [17]$$

where the scalars α and β are undetermined functions of the scalar invariants of the system, and are to be modeled. Internal equilibrium requires that

$$\alpha = -\beta. \qquad [18]$$

While [16] and [17] are a formal consequence of the admissible list of variables, one cannot overlook the physical assumption made at this point. Indeed, if the equations are applied to the simple case of a stiff porous medium at rest, the simple balance between the pressure gradient and the permeability,

$$\frac{\partial \Pi}{\partial x^i} = -\alpha v_j, \qquad [19]$$

shows that the fluid velocity is aligned with the pressure gradient, with a proportionality factor independent of direction. This can only be true if the principal directions of the initial metric coincide with those of the Darcy permeability matrix, with the length of the axes such that the permeability can be characterized by a single scalar (all eigenvalues equal).

Thus it becomes apparent that the choice of axes at the upstream section is implicitly made in the list of variables leading to [16] and [17]. The principal directions of the permeability matrix can be safely assumed to be parallel and perpendicular to the face of the sheet. The length of the basis vectors must be adjusted so that the parameter α is the same in both directions. Thus, the axes are completely determined (up to a scaling factor) at the upstream end. This point will be used in the discussion of the boundary conditions (section 6).

Besides α, another parameter must be introduced in relation to the boundary conditions. When integrated over a surface element, the total pressure (say) acts partly on the fibers and partly on the water. Following Biot (1955), let us introduce the porosity f of the fiber mat as the measure of the ratio of nonsolid areas to solid areas in a section of the material:

$$f = \frac{A_w}{A_f}; \qquad [20]$$

A_w stands for the area occupied by water and A_f for that occupied by fibers. It is assumed that the porosity does not depend on the orientation of the section. Stresses at the boundaries will be calculated by weighing the single-phase stresses according to the corresponding areas of contact.

The modeling of the two parameters α and f can now be addressed. Both are related to the deformation of the mat, i.e. either to g or γ. Strictly speaking, scalar functions such as α and f will depend on all the scalar invariants of the metric tensor. The simplifying assumption is introduced that only the determinant (first invariant) needs to be considered; i.e. we assume that α and f depend on g only. The experimental results of Ceckler & Thompson (1982), presented in figure 2, correspond approximately to the power law

$$\alpha = Ag^{-2.75}, \qquad [21]$$

where the parameter A varies from material to material, and can be determined experimentally. This relation may have to be linearized for computational convenience.

The relation between the porosity f and the parameter g must also be established. Under the condition of isotropy of the porosity, it can be shown (e.g. Bedford & Drumheller 1983) that it is directly related to the phase fractions. With our definition of porosity, we have:

$$f = \phi(1 - \phi), \qquad [22]$$

where the phase fraction of water (per volume) can be calculated directly from the local metric, the compression of the solid and the upstream water content. At the upstream boundary, a relative volume fraction of water can be given as ϕ_0, and the determinant of the metric tensor as g_0. It is well-known that this determinant measures the volume element based on the local base vectors. Then, the volume constructed on the base vectors contains a volume $(1 - \phi_0)g_0$ of solid. If we neglect the compressibility of the solid itself (only allowing for a change in apparent volume due to the expulsion of water from the saturated medium), the definition of the coordinate system ensures that the same volume of solid is contained after strain. Thus, the volume fraction of water after strain is

$$\phi = 1 - (1 - \phi_0)\left(\frac{g_0}{g}\right)^{1/2}, \qquad [23]$$

where it is understood that ϕ must satisfy the condition

$$0 < \phi < 1. \qquad [24]$$

Combining these expressions gives the model for the porosity under the form

$$f = \frac{g - (1 - \phi_0)g_0}{(1 - \phi_0)g_0}. \qquad [25]$$

Finally, the total pressure is obtained by adding, in proportion to the respective porosities, the hydraulic and solid pressures acting on any control surface (e.g. Flügge 1972). Thus,

$$\text{total pressure} = (1-f)\cdot\Pi + f\pi. \qquad [26]$$

Having ascertained that viscous terms do not introduce new unknowns (only material parameters such as μ and μ_s), the viscous forces will be ignored in the remainder of this paper. Two more elements should be introduced before substitution in the general equations of motion. We assume (subject to eventual confirmation from numerical results) that the convective terms in the water equation are due mostly to the convection by the mat itself, and that a linear approximation for the relative momentum equation would be adequate. Thus, we define

$$U^k = v^k - u^k \qquad [27]$$

for the relative velocity of the water in the fiber mat, and ignore terms quadratic in U.

Finally, full advantage is taken of the choice of metric at the upstream end. As discussed in section 2, the unknown boundary of the fiber mat can be taken to be a coordinate surface, and a streamline for the flow of porous solid. Hence, one entire family of coordinate lines (in the plane of the flow) can be made of streamlines, so that two of the velocity components for the solid flow would vanish identically. Thus, we can begin to define the coordinate system by the equations

$$u^2 = u^3 = 0. \qquad [28]$$

Furthermore, with the other coordinate surfaces as timelines, the first component of velocity is constant, and

$$u^1 = V. \qquad [29]$$

Equations [28] and [29] merely express the fact that the flow of solid material generates the local base vectors. Rather than having variable velocities in a cartesian coordinate system, we have uniform flow in a variable metric. The flow problem has been reduced to finding the coordinate system in which the flow of solid material is uniform. For a chosen time interval, the spacing of the streamlines at the upstream boundary completes the coordinate system.

It follows that the continuity equation [3] for the fibers is automatically satisfied. For convenience, the x^1 (streamwise) coordinate will be written as "t" and the cross-stream coordinate x^2 as "z". Equations [6] and [7] can be spelled out as

$$\frac{\partial U^1}{\partial t} + \frac{\partial U^2}{\partial z} + U^1\Gamma^k_{k1} + U^2\Gamma^k_{k2} + \Gamma^k_{k1} = 0, \qquad [30]$$

$$\rho\left(\Gamma^1_{11} + \frac{\partial U^1}{\partial t} + \Gamma^1_{11}U^1 + \Gamma^1_{12}U^2 + U^1\Gamma^1_{11} + U^2\Gamma^1_{21}\right) = -Ag^{-2.75}U^1 - \frac{\mathrm{D}\pi}{\mathrm{D}x^1} \qquad [31]$$

and

$$\rho\left(\Gamma^2_{11} + \frac{\partial U^2}{\partial t} + \Gamma^2_{11}U^1 + \Gamma^2_{12}U^2 + U^1\Gamma^2_{11} + U^2\Gamma^2_{21}\right) = -Ag^{-2.75}U^2 - \frac{\mathrm{D}\pi}{\mathrm{D}x^2}, \qquad [32]$$

which can be solved for U^1, U^2 and π once g^{ij} is known, and

$$P\Gamma^1_{11} = Ag^{-2.75}U^1 - \frac{E}{2(1+\nu)}\frac{\nu}{1-2\nu}\left\{g^{11}\frac{\partial}{\partial x^1}(g^{km}g^0_{km}) + g^{12}\frac{\partial}{\partial x^2}(g^{km}g^0_{km})\right\}$$

$$- \frac{E}{2(1+\nu)}\frac{\mathrm{D}}{\mathrm{D}x^j}(g^{1k}g^{jm}g^0_{km}) \qquad [33]$$

and

$$P\Gamma^2_{11} = Ag^{-2.75}U^2 - \frac{E}{2(1+\nu)}\frac{\nu}{1-2\nu}\left\{g^{21}\frac{\partial}{\partial x^1}(g^{km}g^0_{km}) + g^{22}\frac{\partial}{\partial x^2}(g^{km}g^0_{km})\right\}$$

$$- \frac{E}{2(1+\nu)}\frac{\mathrm{D}}{\mathrm{D}x^j}(g^{2k}g^{jm}g^0_{km}) \quad [34]$$

governing the field of g^{ij}s together with the definition [2] of the Γs, the compatibility equation [15], and with "D" denoting the covariant derivative. The reference metric at a given location, serving in the definition of the strains, is calculated as follows.

With the length of the streamwise axis taken as proportional to the streamwise velocity V, the anisotropy defines the length of the e_2 axis as a. The spanwise axis can be taken as an arbitrary constant under the two-dimensional flow assumption, and will be ignored in the following. Hence, the initial metric tensor is of the form

$$(g_{ij}|_{t=0}) = \begin{pmatrix} V^2 & 0 \\ 0 & a^2 \end{pmatrix} \quad \text{with } g = V^2a^2. \quad [35]$$

As the material is convected, the deformation can be decomposed into a rotation and a pure strain applied to the initial metric [35]. In matrix notations, we can write

$$\mathbf{g} = \mathbf{S}^{\mathrm{T}}\mathbf{R}^{\mathrm{T}}\mathbf{g}|_{t=0}\mathbf{R}\mathbf{S}, \quad [36]$$

where **S** and **R** stand for the straining and rotation matrices, respectively. When we call λ_1 and λ_2 the eigenvalues of the metric tensor,

$$\lambda_1 = \tfrac{1}{2}[g_{11} + g_{22} + \sqrt{(g_{11}-g_{22})^2 + 4g_{12}^2}]$$
$$\lambda_2 = \tfrac{1}{2}[g_{11} + g_{22} - \sqrt{(g_{11}-g_{22})^2 + 4g_{12}^2}], \quad [37]$$

the matrices **S** and **R** can be calculated easily:

$$\mathbf{S} = \begin{bmatrix} \dfrac{\sqrt{\lambda_1}}{V} & 0 \\ 0 & \dfrac{\sqrt{\lambda_2}}{a} \end{bmatrix} \quad [38]$$

and

$$\mathbf{R} = \begin{bmatrix} \dfrac{g_{12}}{\sqrt{(\lambda_1-g_{11})^2+g_{12}^2}} & \dfrac{\lambda_2-g_{22}}{\sqrt{(\lambda_1-g_{22})^2+g_{12}^2}} \\ \dfrac{\lambda_1-g_{11}}{\sqrt{(\lambda_1-g_{11})^2+g_{12}^2}} & \dfrac{g_{12}}{\sqrt{(\lambda_2-g_{22})^2+g_{12}^2}} \end{bmatrix}$$

$$= \begin{bmatrix} \dfrac{g_{12}}{D} & \dfrac{\lambda_2-g_{22}}{D} \\ \dfrac{\lambda_1-g_{11}}{D} & \dfrac{g_{12}}{D} \end{bmatrix}. \quad [39]$$

At any point, the reference metric g^0_{ij} is defined as that corresponding to local coordinates obtained by relaxing the stresses locally: in the principal axes of the tensor g_{ij}, this amounts to relaxing the normal stresses. Thus, g^0_{ij} is obtained by rotating the initial metric into the principal directions of g_{ij}. Thus,

$$(g^0_{ij}) = \begin{bmatrix} \dfrac{g_{12}}{D} & \dfrac{\lambda_1-g_{11}}{D} \\ \dfrac{\lambda_2-g_{22}}{D} & \dfrac{g_{12}}{D} \end{bmatrix} \begin{pmatrix} V^2 & 0 \\ 0 & a^2 \end{pmatrix} \begin{bmatrix} \dfrac{g_{12}}{D} & \dfrac{\lambda_2-g_{22}}{D} \\ \dfrac{\lambda_1-g_{11}}{D} & \dfrac{g_{12}}{D} \end{bmatrix}$$

or

$$(g^0_{ij}) = \begin{bmatrix} \dfrac{a^2(\lambda_1 - g_{11})^2 + V^2 g_{12}^2}{(\lambda_1 - g_{11})^2 + g_{12}^2} & \dfrac{(V^2 - a^2) g_{12}(\lambda_1 - g_{11})}{(\lambda_1 - g_{11})^2 + g_{12}^2} \\ \dfrac{(V^2 - a^2) g_{12}(\lambda_1 - g_{11})}{(\lambda_1 - g_{11})^2 + g_{12}^2} & \dfrac{V^2(\lambda_1 - g_{11}) a^2 g_{12}^2}{(\lambda_1 - g_{11})^2 + g_{12}^2} \end{bmatrix} \quad [40]$$

is known at every point, if the metric tensor is.

In this approximation, we have reduced the problem of wet pressing to a system of 6 partial differential equations for the 6 unknowns U^1, U^2, π, g_{11}, g_{12} and g_{22}. The model parameters A, B, E and ν (together with μ and μ_s if viscosity is kept in the model) and the exponent in [21] are all material constants and can be determined experimentally. Thus, the system of equations [30]–[34] can be solved in principle, if the boundary conditions are provided (section 6).

5. MAPPING TO CARTESIAN COORDINATES

Having obtained a solution for **U** and **g**, the presentation of the results will best be done in "laboratory" (cartesian) coordinates. The problem can be formulated as follows: knowing the g_{ij}s at every point of the deformed plane, calculate the equation of the streamlines and timelines in the laboratory coordinates, i.e.

$$\left.\frac{\partial y}{\partial x}\right|_z = \phi(g_{ij}) \quad [41]$$

and

$$\left.\frac{\partial x}{\partial y}\right|_t = \psi(g_{ij}), \quad [42]$$

respectively. The Jacobian of the change of coordinates $(x, y) \rightarrow (t, z)$ is defined by the relation

$$\begin{pmatrix} dx \\ dy \end{pmatrix} = \begin{bmatrix} \left.\dfrac{\partial x}{\partial t}\right|_z & \left.\dfrac{\partial x}{\partial z}\right|_t \\ \left.\dfrac{\partial y}{\partial t}\right|_z & \left.\dfrac{\partial y}{\partial z}\right|_t \end{bmatrix} \begin{pmatrix} dt \\ dz \end{pmatrix} = \begin{pmatrix} J_{11} & J_{12} \\ J_{12} & J_{22} \end{pmatrix} \begin{pmatrix} dt \\ dz \end{pmatrix}. \quad [43]$$

By definition of the metric tensor g_{ij}, we also have

$$dx^2 + dy^2 = g_{11}\, dt^2 + 2g_{12}\, dt\, dz + g_{22}\, dz^2. \quad [44]$$

It follows that

$$\begin{pmatrix} J_{11} & J_{21} \\ J_{12} & J_{22} \end{pmatrix} \begin{pmatrix} J_{11} & J_{12} \\ J_{21} & J_{22} \end{pmatrix} = \begin{pmatrix} g_{11} & g_{12} \\ g_{21} & g_{22} \end{pmatrix}. \quad [45]$$

The problem is solved if we can calculate the components of the Jacobian. The matrix equation [45] can be rewritten as the system of scalar equations

$$\begin{aligned} J_{11}^2 + J_{21}^2 &= g_{11} \\ J_{11} J_{12} + J_{21} J_{22} &= g_{12} \\ J_{12}^2 + J_{22}^2 &= g_{22}. \end{aligned} \quad [46]$$

The symmetry of the metric tensor results in an indeterminate system: taking J_{11} as reference, the other elements can be calculated as

$$J_{21} = \pm(g_{11} - J_{11}^2)^{1/2}, \quad [47]$$

$$J_{12} = \frac{J_{11} g_{12}}{g_{11}} \pm \frac{1}{g_{11}} [(g_{11} - J_{11}^2)(g_{11} g_{22} - g_{12}^2)]^{1/2} \quad [48]$$

and

$$J_{22} = \pm\frac{J_{11}g^{1/2}}{g_{11}} \pm \frac{g_{12}}{g_{11}}(g_{11} - J_{11}^2)^{1/2}. \tag{49}$$

The elements of the Jacobian are further constrained by their own symmetry conditions, which arise from the commutativity of second partial derivatives:

$$\frac{\partial}{\partial z}\frac{\partial x}{\partial t} = \frac{\partial J_{11}}{\partial z} = \frac{\partial J_{12}}{\partial t} = \frac{\partial}{\partial t}\frac{\partial x}{\partial z} \tag{50}$$

and

$$\frac{\partial}{\partial z}\frac{\partial y}{\partial t} = \frac{\partial J_{21}}{\partial z} = \frac{\partial J_{22}}{\partial t} = \frac{\partial}{\partial t}\frac{\partial y}{\partial z}. \tag{51}$$

When the Js are related through the metric tensor as above, it can be shown from the definition of the J_{ij}s, that these two equations are equivalent. Thus, with the components of the metric tensor known, the last element of the Jacobian must obey the relation

$$\frac{\partial J_{11}}{\partial z} = \frac{\partial}{\partial t}\left\{\frac{J_{11}g_{12}}{g_{11}} \pm \frac{1}{g_{11}}[(g_{11} - J_{11}^2)(g_{11}g_{22} - g_{12}^2)]^{1/2}\right\}, \tag{52}$$

subject to the upstream boundary condition that $J_{11} = V$.

Hence, it follows from the theory of Jacobians that

$$\left.\frac{\partial y}{\partial x}\right|_z = \frac{J_{21}}{J_{11}} = \pm\frac{(g_{11} - J_{11}^2)^{1/2}}{J_{11}} \tag{53}$$

is the equation of the streamlines in the laboratory coordinates, with J_{11} given by the solution of [52]. Similarly, the timelines are given by

$$\left.\frac{\partial x}{\partial y}\right|_t = \frac{J_{12}}{J_{22}}. \tag{54}$$

It should be noted that a given field of strain (metric tensor) must satisfy a compatibility condition, if the deformed configuration is to be obtained by a regular mapping from the reference configuration. The existence of continuously differentiable elements of the Jacobian, ensures that such a mapping $(x, y) \rightarrow (t, z)$ does exist. Hence, the compatibility equation will automatically be satisfied.

6. BOUNDARY CONDITIONS

Equations [30]–[34] have to be solved on a rectangular grid in the t–z plane. Several types of boundary conditions will have to be applied along sections of the boundaries. The entrance ($t = -\tau$) and exit ($t = \tau$) sections are assumed to be far enough away from the nip for the direct effect of the rolls to be negligible. Thus, $t = -\tau$ corresponds to the equilibrium initial conditions; at $t = \tau$, the properties of the mat have also relaxed to equilibrium, with possibly a different thickness, anisotropy and/or velocity of the mat.

For simplicity, $t = 0$ is located at the center of the contact area of the mat with the rolls. In the absence of a fiber mat, symmetry about the mat centerline indicates that the half-thickness plane will not be bent in the press, and provides a convenient axis $z = 0$. Call $z = \zeta$ the face of the paper sheet.

Let $t = \pm\theta$ be the entrance and exit coordinates of the outer surface at the nip. The length of the interval $[-\theta, +\theta]$ is an experimental control parameter, to the extent that it will depend on the force applied by the rolls on the sheet. Inside the interval, the face of the sheet must match the cylindrical shape of the rolls, so that the curvature of the boundary streamlines is imposed. As pointed out by one of the reviewers of this paper, imposing such a boundary condition leads to an ill-posed problem. Practically, a pressure profile can be imposed on the solid, the

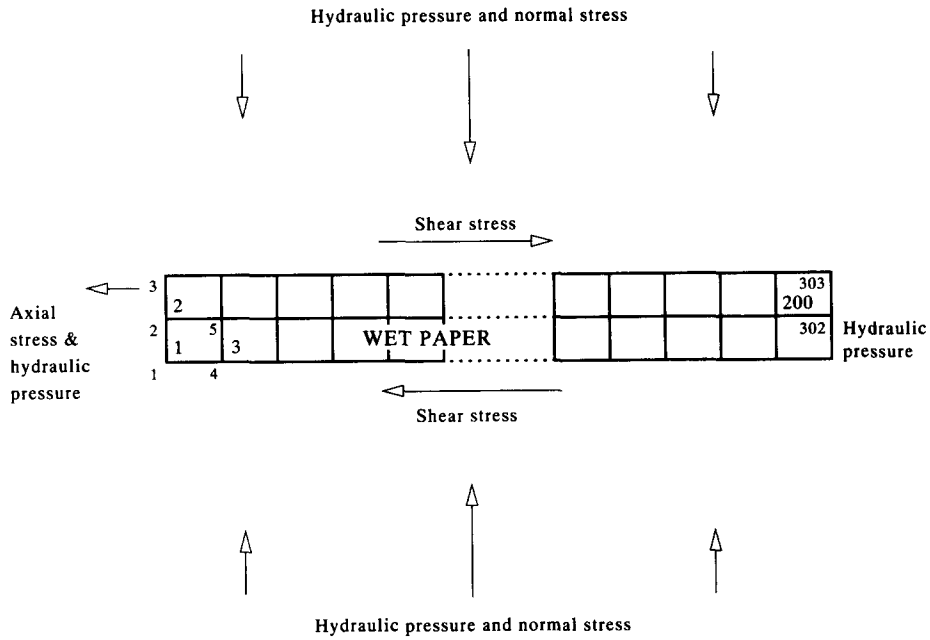

Figure 4. Hydraulic pressure and normal stress.

corresponding solution calculated and the shape of the boundary adjusted by trial and error until a cylindrical streamline is obtained.

In practice, one of the rolls is driven and imposes a shear stress on the face of the sheet, while the opposite roll drags on the opposite side. The applied shear stress can be modeled by Coulomb's law of friction, with the proportionality constant between the normal and tangential stresses modeling the degree of lubrication between the pulp and the roll.

With this in mind, the boundary conditions can be listed systematically, and are summarized in figure 4.

At the upstream section ($t = -\tau$), the metric tensor is imposed as in [35]. The magnitude of V can be varied to simulate a range of conditions. Experimental values of the anisotropy can be introduced to initialize "a". With the upstream section sufficiently removed from the rolls, the water is simply carried in the fibers without any relative motion. The simplest assumption on the normal stresses is that no traction is applied in the direction of motion. This sets the reference metric tensor;

$t = -\tau$ and $0 < z < \zeta$:

$$U^1 = U^2 = 0, \quad g_{11} = V^2, \quad g_{22} = a^2, \quad g_{12} = g_{21} = 0, \quad g^0_{ij} = g_{ij}. \tag{55}$$

At the downstream section ($t = \tau$) conditions are similar, except that a number of properties are not known *a priori*. The fiber mat is not necessarily moving at the same velocity as at the upstream end. Anisotropy has to be calculated, and is related to the residual stresses through the metric tensor. All quantities will have relaxed to the new equilibrium values;

$t = \tau$ and $0 < z < \zeta$:

$$U^1 = U^2 = 0, \quad \frac{\partial g_{ij}}{\partial t} = 0. \tag{56}$$

Along the plane of symmetry ($z = 0$), the normal water velocity must vanish, and there cannot be a tangential stress;

$z = 0$ and $-\tau < t < \tau$:

$$U^2 = 0, \quad T^{12} + f\tau^{12} = 0. \tag{57}$$

The stresses in the above are calculated from the constitutive equations; τ^{12} vanishes if the water viscosity is neglected.

Along the face of the sheet downstream of the rolls, one would expect that the normal water velocity would vanish. No stresses are applied on the boundary;

$t > \theta$ and $z = \zeta$:

$$U^2 = 0, \quad T^{12} + f\tau^{12} = 0, \quad T^{11} + f\tau^{11} = 0. \tag{58}$$

Upstream, the situation is similar in many ways, except that water is being forced out. Then, the normal velocity of the water results from the differences in hydraulic pressure between the solution inside the domain and ambient pressure (zero) at the boundary. Non-negative outward normal velocities should follow in order for the solution to be believable, although we do not know *a priori* where the normal velocity would vanish and where it is positive;

$t < -\theta$ and $z = \zeta$:

$$\pi = 0, \quad T^{12} + f\tau^{12} = 0, \quad T^{11} + f\tau^{11} = 0. \tag{59}$$

In the above, π is given by [26] and [14].

The boundary conditions under the rolls have been discussed in the introduction to this section. Assuming impermeable rolls, no normal water velocity will be allowed; the normal water pressure gradient is given by [32] accordingly. For the metric tensor, two conditions are imposed;

$-\theta < t < \theta$ and $z = \zeta$:

$$U^2 = 0, \quad \left.\begin{matrix} T^{12} + f\tau^{12} \\ T^{22} + f\tau^{22} \end{matrix}\right\} \text{ assumed distribution/magnitude.} \tag{60}$$

7. DISCUSSION

The equations and boundary conditions derived above are a complement to empirical studies. From the experimentalist's perspective, the weak points of this approach must be glaring: we shall attempt to address some of them. On the other hand, the rigorous mathematical treatment, based on the methods of rational mechanics and well-documented phenomenological approximations, can provide a different insight into a complex industrial process such as wet pressing. All control parameters (mat velocity, nip pressure, mat thickness, driving power, roll radius), as well as the material constants, can be modified systematically and accurately. Qualitative effects of mat rheology can also be documented. A numerical solution such as is presented in section 8 should be regarded as a controlled experiment, with simplifications in configuration being balanced by the accuracy of the "measurement" of all variables in the flow field.

Based on those observations, extensions of the model to more realistic conditions can be anticipated. First and foremost (and probably easiest) will be the introduction of the felt mat. While the numerical constants for the felt (thickness, porosity, mechanical properties etc.) are different from those of the paper sheet, the basic equations remain unchanged. The loss of symmetry in the z direction, and the matching of solutions at the paper–felt interface, do not seem to pose an overwhelming difficulty. However, for a realistic description of an actual press, it is necessary to account for the fact that the felt will not be nearly saturated upstream of the nip—and that neither the felt nor the paper will be on the downstream side. In fact, two fluids percolate through the porous mats: air and water. The simplest representation of the two fluid phases is that they remain separated by a sharp interface, the location of which has to be determined. The paper of Thigpen & Berryman (1985) provides the framework to extend our results, when the interphase forces are parameterized by pressure jumps and capillary forces at the air–water interface. Finally, the compliance of the rolls appears experimentally significant. Again, this is a relatively simple question of matching two solutions: all stresses in the nip region of both rolls, the paper and the felt, must balance locally.

To this extent, the material presented in this article truly represents a first step in the direction of a better analytical understanding of the wet pressing process. The numerical solution of the equations in the next section exposes both merits and weaknesses of this approach.

8. NUMERICAL IMPLEMENTATION

Experimentally, severe limitations are encountered in the nature and accuracy of the measurements. The residence time in commercial nips is of the order of 0.001–0.002 s. The press nips are about 1" long with a paper thickness of the order of 0.01". Therefore, the selection of the measured field variables is dictated more by feasibility than by the need for physical insight, and the documentation of the flow field is rudimentary. The numerical simulation has its own limitations, as seen below, but it must be considered successful if it accounts for empirical observations of changes in the system response under changes in the control parameters. Then, the computed flow field is a valuable surrogate measurement.

Our model system consists of a sheet of water-saturated pulp being drawn between two cylindrical hard rolls. The single layer of porous pulp is modeled as elastic. The viscosity of the water is neglected, except insofar as its macroscopic effect manifests itself as Darcy's law for fluid–solid interaction. The friction between the rolls and the sheet follows Coulomb's model. Air is not allowed into the pulp during recovery downstream of the nip.

The system of equations [30]–[34] has been solved by the Galerkin finite-element method. The field variables are approximated locally as polynomials of the nodal values, that are adjusted to minimize the residual in the equations. The procedure results in an algebraic system of equations for the nodal values. The system of equations contains 6 primary variables at each node (3 components of the metric tensor for the solid and 2 velocity components and the pressure for the water). The variables occur in products including as many as 5 factors. The computation of all combinations of these products is prohibitively time-consuming.

A reduction in the number of factors in a product can be done by introducing secondary variables, for which the governing equations are the respective definition formulas. The increase in the number of equations results in a decrease in the computation time to establish the system matrix, and an increase in the number of iterations for each system. Numerical experimentation showed that the elimination of all products of more than 2 factors is most effective. The definitions of the secondary variables are listed as [B7]–[B28] and substitution of these definitions in [30]–[34] yields [B1]–[B6] in appendix B.

Three nested iterative procedures define the code structure. At the core of the algorithms, the Galerkin finite-element method converts the set of partial differential equations to a set of algebraic equations. The successive over-relaxation (SOR) method is used to solve these algebraic equations. The outermost iterations consist of using the new solution as the initial condition, incrementing the load and repeating the process described above. Finite deformations are obtained by incremental increases in load.

Linear shape functions are chosen for interpolation within the finite elements. This choice is dictated by the large number of terms and unknowns, which make everything but the simplest shape function prohibitively time-consuming. Furthermore, since the equations have, at most, first-order differentiations of variables, the C_0 continuity of the linear shape functions is sufficient. Because of the dependence of the solution on the current solution, which differs from element to element, the local residual equations have to be constructed at each iteration.

The global matrix is stored in a banded format to take advantage of its structure. The boundary conditions are applied next, replacing the residual equations corresponding to given variables at the boundary nodes by equalities fixing the value of the specified variables at the nodes. The global matrix is further conditioned by a partial pivoting routine to allow the larger elements to be on the diagonal.

The SOR procedure was used to solve the set of equations developed as above. This procedure minimizes the possibility of accumulation of roundoff errors, resulting in divergence from the solution. A small relaxation parameter of 0.01 had to be used to achieve convergence. After obtaining a solution for the increments, a new current solution is formed and the residual equations

are constructed to iterate the solution. This iterative process is contained until convergence is obtained within a tolerance level of 10^{-6}.

Experimentation with meshes revealed that solution gradients in the thickness direction were negligible, in contrast to the large axial gradients direction. Hence, the solutions in the following section were obtained using a finite-element mesh consisting of only 2 elements in the thickness direction and 100 elements in the axial direction (see figure 1). The calculations were limited to the nip area. The boundary conditions consisted of the applied tractions on the boundaries as well as Dirichlet conditions on the hydraulic pressure along the boundary.

9. DESCRIPTION AND SOLUTIONS FOR CASE STUDIES

Pressure-controlled and flow-controlled pressing are important extreme cases often cited in the literature (Wahlstrom 1960, Jewett 1984, Nilsson 1964, Wilder 1967). Pressure-controlled pressing results when the permeability is very high. In this case the removal of water is limited by the amount of compression possible for a given amount of applied stress. In terms of the parameters used in the calculations, α ([19]), the coefficient of the body force in the momentum balance equations which is inversely related to the permeability, is small. On the other hand, flow-controlled pressing results when the removal of water is limited by the flow resistance of the material or the permeability is small. Correspondingly, the value of α is large.

These first two case studies help develop confidence in the model results. As discussed earlier, the respective limitations of the experimental and computational approaches preclude any strict experimental verification in the near future. However, the trends in the numerical results are in agreement with observations. Following this, the third case study demonstrates the utility of our approach in predicting important consequences of the presence, absence and direction of shear stress gradients across the thickness of the sheet.

A normal load of 1.7×10^6 N/m^2 was applied in the first two cases, while a load of 5.1×10^5 N/m^2 was applied for the third case study. This resulted in a maximum strain of about 17% in the thickness direction for cases 1 and 2, and a strain of about 5% for case 3. The values of the various parameters used in the flow-controlled case are listed in table 1, while those used in the pressure-controlled case are listed in table 2.

The results are presented in the form of two graphs per solution. The first figure plots the fluid-phase pressure, or hydraulic pressure, and the total stress tensor components against the distance along the nip. The total stress tensor includes both the solid- and fluid-phase stresses. The distance along the nip is measured from the point at which the sheet enters the press nip. The other figure plots the axial (machine) direction and transverse (thickness) direction water velocities at the three levels along the nip. In both these figures, the values of the lowest level of nodes are

Table 1. Parameters used in the flow-controlled case

Resistance to the flow of water, α	5.0×10^{10} N s/m^4
Corresponding permeability	2.5×10^{-15} m^2
Water velocity at roll surfaces	0 m/s
Gradient of Al w.r.t. to g, α'	0.25×10^{10} N s/m^4
Hooke's coefficient, E	1×10^7 N/m^2
Gradient of E w.r.t. to g, E'	0.25×10^7 N/m^2
Poisson's ratio	0.05
Thickness of the ingoing sheet	0.5 mm
Velocity of the fiber matrix in the machine direction	0.5 m/s
Normal stress at the left edge	0 psi
Normal stress at the nip center	200 psi
Normal stress at the right edge	0 psi
Normal stress gradient on the left and right edges	0 psi
Axial stress at the left edge	50 psi
Shear stress at the bottom	−15 psi
Shear stress at the top	−10 psi

Table 2. Parameters used in the pressure-controlled case

Resistance to the flow of water, α	5.0×10^8 N s/m^4
Corresponding permeability	2.5×10^{-13} m^2
Hydraulic pressure at the sheet–felt interface	0 psi
Gradient of Al w.r.t. to g, α'	0.25×10^{10} N s/m^4
Hooke's coefficient, E	1×10^7 N/m^2
Gradient of E w.r.t. to g, E'	0.25×10^7 N/m^2
Poisson's ratio	0.05
Thickness of the ingoing sheet	0.5 mm
Velocity of the fiber matrix in the machine direction	0.5 m/s
Normal stress at the left edge	0 psi
Normal stress at the nip center	200 psi
Normal stress at the right edge	0 psi
Normal stress gradient on the left and right edges	0 psi
Axial stress at the left edge	50 psi
Shear stress at the bottom	−15 psi
Shear stress at the top	−10 psi

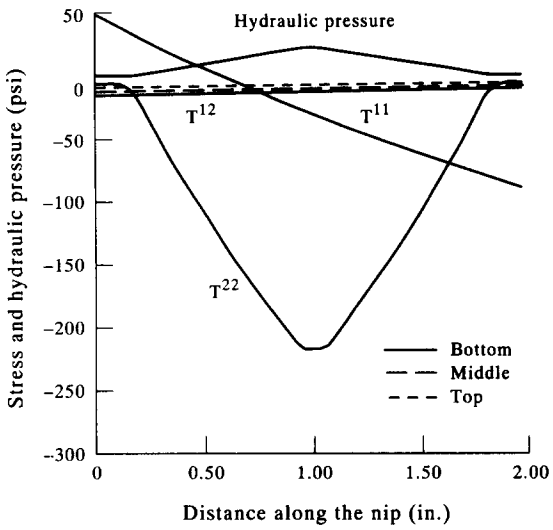

Figure 5. The stress tensor components and the hydraulic pressure vs the distance along the nip, for the pressure-controlled pressing case.

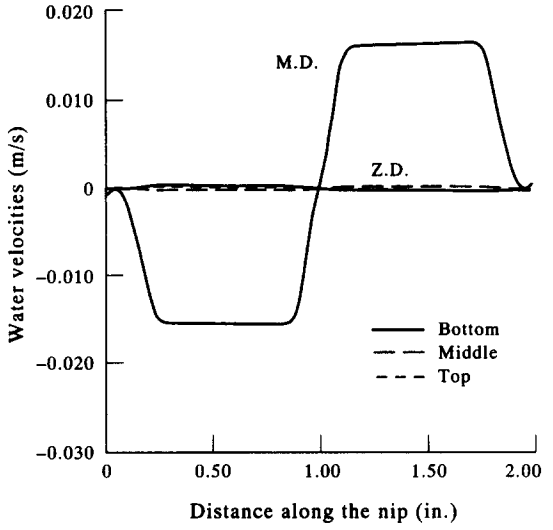

Figure 6. The machine and transverse direction water velocities vs the distance along the nip, for the pressure-controlled pressing case.

connected by the —— line, the values along the top surface by the ---- line and the values along the middle are connected by the ——— line.

The pressure-controlled case results are presented in figures 5 and 6. Figure 5 shows that the gradients for the stress tensor components and the hydraulic pressures are minimal in the thickness direction, causing a superposition of several of the lines. A gradient in the shear stress component is imposed by the boundary conditions for traction, which causes the drop in the axial stress along the nip. This phenomenon is further explained later. It is to be noted that the hydraulic pressure attains a maximum at the center of the nip, where the maximum normal stresses are imposed, for this pressure-controlled situation.

The axial and transverse water velocities for this pressure-controlled case are shown in figure 6. The gradients in the thickness direction are small and the water velocities in the thickness direction are negligible. The machine direction velocities show that water is pushed out axially from the center of the nip with equal velocities. The maximum velocity is attained close to the center of the nip and then the water progresses to exist from both sides of the nip. The assumption of elastic behavior for the pulp allows the pulp to spring back to its original shape as the normal stresses are released. This causes the results to be symmetrical around the center of the nip, as a consequence of the assumptions of elastic material and boundary conditions.

Figure 7 presents the stress tensor components and the hydraulic pressure along the nip for this case of flow-controlled pressing. The maximum hydraulic pressure in this case is attained early on in the nip, for upstream of the center point of the nip. Figure 8 shows that this causes the axial water velocity to be relatively small for most of the nip, with a strong outward flow in the initial part of the nip. A negative hydraulic pressure is developed towards the end of the nip, causing an inflow of water into the nip. This tendency was absent for the pressure-controlled case. The absolute values of the water velocities are much lower than in the pressure-controlled case, in accordance with the much lower permeability. The thickness direction water velocities are negligible as before, due to small gradients in the hydraulic pressure in that direction.

As a third case, the effect of imposed shear stress was studied with a smaller number of elements. Two elements were used in the thickness direction, as before, but the number of elements in the axial direction was reduced to 23. The computation time is significantly less, while the accuracy of the solution is off by a few percent. Four sets of conditions were examined:

(a) Zero shear stress at all nodes.
(b) Constant negative shear stress at all nodes.
(c) A positive shear stress gradient in the thickness direction.
(d) A negative shear stress gradient in the thickness direction.

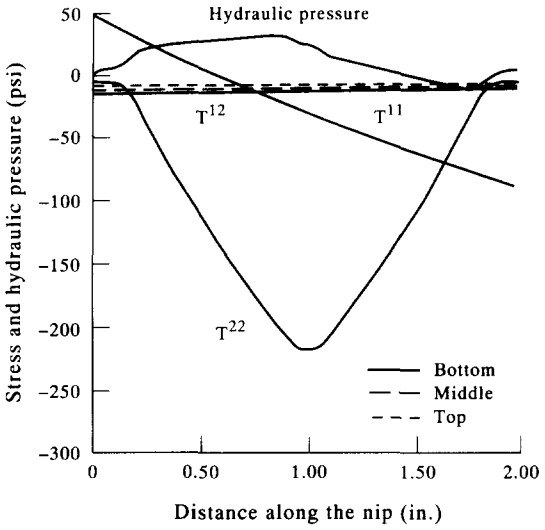

Figure 7. The stress tensor components and the hydraulic pressure vs the distance along the nip, for the flow-controlled pressing case.

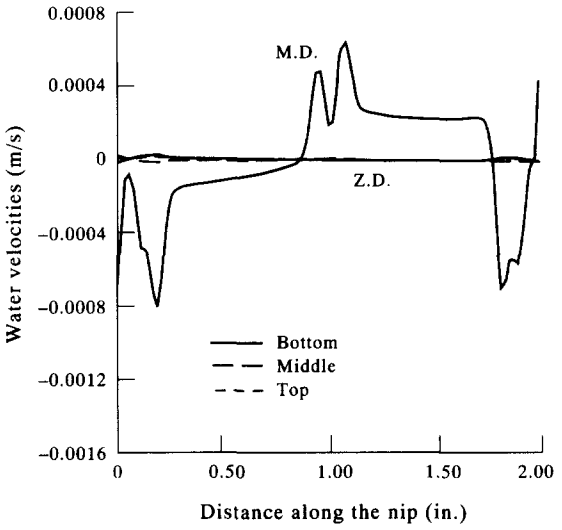

Figure 8. The machine and transverse direction water velocities vs the distance along the nip, for the flow-controlled pressing case.

The exact nature of the shear stresses in the real press is not known because it is extremely difficult to measure them. Hence, the stress distributions applied in this study are estimates derived from Coulomb's laws of friction. The paper–roll interface cannot be frictionless, which leads one to infer that frictional forces equal to some coefficient of friction times the normal stress will prevail at the interface.

The direction of these frictional forces, or shear stresses, depends on the press roll's velocity relative to the sheet of pulp and also on the roll surface's coefficient of friction with the pulp. If the bottom roll is driven and the top roll is not (as is usually the case) and if both rolls have the same coefficient of friction (which is usually not the case), a constant negative shear stress will prevail throughout the sheet. On the other hand, if the top roll has a higher coefficient of friction than the lower roll, a positive shear stress gradient will be set up in the sheet. Similarly, a negative shear stress gradient will exist if the top roll has a lower coefficient of friction than the lower roll.

Table 3. Parameters used for the study of the effect of the shear stress and the shear-stress gradient

Resistance to the flow of water, α	1.0×10^{10} N s/m^4
Corresponding permeability	1.245×10^{-14} m^2
Water velocity at roll surfaces	0 m/s
Gradient of Al w.r.t. to g, α'	0.25×10^{10} N s/m^4
Hooke's coefficient, E	1×10^7 N/m^2
Gradient of E w.r.t. to g, E'	0.25×10^7 N/m^2
Poisson's ratio	0.05
Thickness of the ingoing sheet	0.5 mm
Velocity of the fiber matrix in the machine direction	0.5 m/s
Normal stress at the left edge	0 psi
Normal stress at the nip center	38 psi
Normal stress at the right edge	0 psi
Normal stress gradient on the left and right edges	0 psi
Axial stress at the left edge	50 psi

Four sets of shear stress conditions were used: (a) shear stress at all nodes 0 psi; (b) shear stress at all nodes −15 psi; (c) shear stress at the bottom = −15 psi, shear stress at the top = −8 psi; (d) shear stress at the bottom = −16 psi, shear stress at the top = −22 psi.

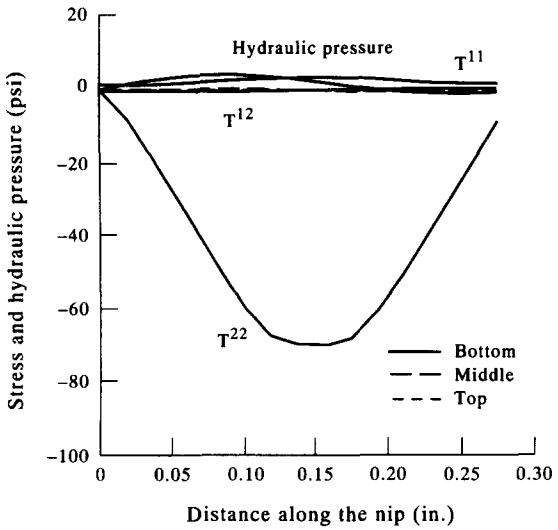

Figure 9. The stress components and the hydraulic pressure vs the distance along the nip, for the case when the shear stress is zero at all nodes.

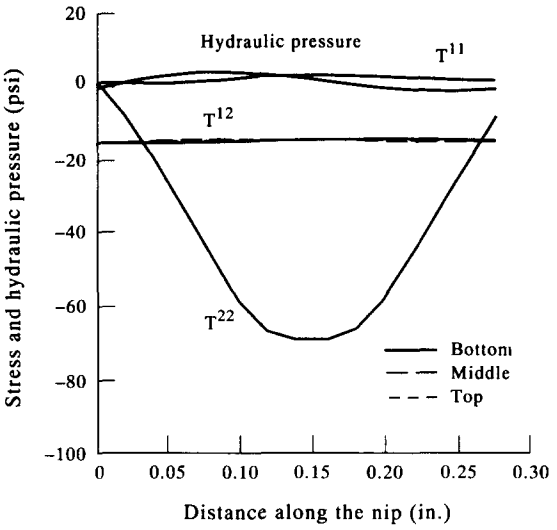

Figure 10. The stress tensor components and the hydraulic pressure vs the distance along the nip, for the case when the shear stress is negative at all nodes.

The values of the various parameters used in the 4 sets of conditions for this third case study are listed in table 3.

Figures 9–12 present the stress tensor components and hydraulic pressure for these 4 cases. It is seen that the axial stresses are not affected for constant-negative or zero shear stresses at all nodes. However, the axial tensile stresses decreased along the machine direction for a positive shear-stress gradient in the thickness direction, while they increased for the case of a negative shear-stress gradient in the thickness direction.

We may infer that if the top surface of the paper sheet has a higher shear stress than the bottom surface, due to, for example, a higher coefficient of friction with the top roll, the tensile forces in the sheet will decrease along the nip. This will result in a smaller volume of material coming out of the nip, implying a higher dewatering rate. Since dewatering is an important objective of wet pressing, this result is of practical significance.

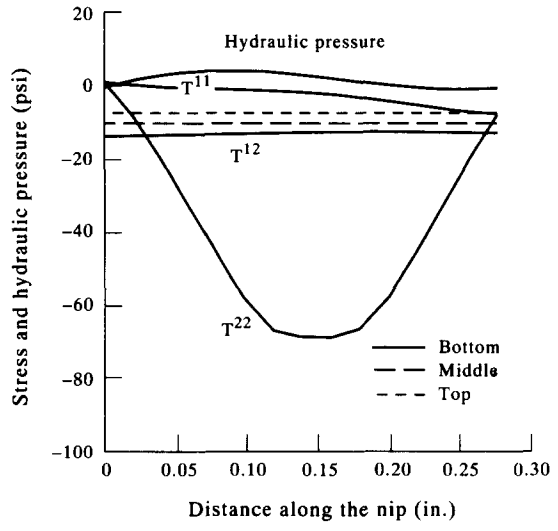

Figure 11. The stress tensor components and the hydraulic pressure vs the distance along the nip, for the case when the shear stress gradient is positive along the transverse direction.

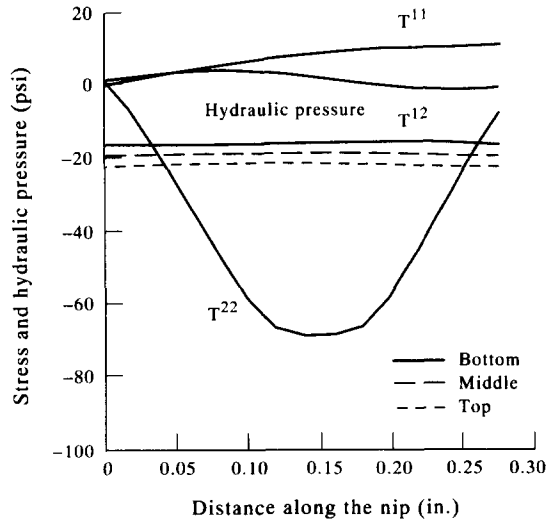

Figure 12. The stress tensor components and the hydraulic pressure vs the distance along the nip, for the case when the shear stress gradient is negative along the transverse direction.

10. CONCLUSIONS

In the first part of the article, the equations governing two-dimensional flows in rapidly deforming porous media are obtained in material coordinates. The second part presents numerical results based on these equations.

The use of generalized coordinates provides the level of generality necessary to describe, in principle, the response of layered porous materials and multiphase flows under realistic boundary conditions. However, full exploitation of this potential is limited by the numerics. The large number of nodal variables severely limits the grid resolution. This limitation echoes the shortcomings of experimental approaches to the problem.

The model has provided results consistent with experience and intuition, for example the effect of the permeability on the field variables like the water velocity and hydraulic pressure. It has also provided predictions of the effects of variables that have not yet been investigated, namely the shear stresses and the shear-stress gradients. In conjunction with other methods, the results obtained with this comprehensive approach to modeling of the wet processing process may provide a better understanding of the physics of the process.

Acknowledgements—The authors wish to thank the National Science Foundation, the Empire State Paper Research Institute and the State University of New York, College of Environmental Science and Forestry, who collectively funded this research project. The role of the reference metric and of the compatibility equation was greatly clarified by discussions with Dr A. J. Levy. We are also indebted to Dr R. W. Perkins for urging us to show that viscoelastic materials could be included with little effort. Special thanks are also due to Syracuse University for providing the computing resources on campus, and to the National Center for Supercomputing Applications at the University of Illinois, Urbana-Champaign for the use of a Cray-2 machine.

REFERENCES

ALLEN, M. B. 1985 Mechanics of multiphase fluid flows in variably saturated porous media. *Int. J. Engng Sci.* **24,** 339–351.

BECK, D. A. 1983 Fluid pressures in a press nip: measurements and conclusions. In *TAPPI Engineering Conference Proceedings*, Book 2, pp. 475–487.

BEDFORD, A. & DRUMHELLER, D. S. 1983 Theories of immiscible and structured mixtures. *Int. J. Engng Sci.* **21,** 863–960.

BIOT, M. A. 1955 Theory of elasticity and consolidation for a porous anisotropic solid. *J. Appl. Phys.* **26,** 182–191.

BULLERWELL, P. and BAADE, A. C. 1984 Water removal on high PLI presses. In *TAPPI Engineering Conference Proceedings*, Book 2, pp. 427–437.

CAMPBELL, W. B. 1947 The Physics of Water Removal. *Pulp Paper Mag. Canada* **26,** 103–110.

CARLSSON, G., LINDSTROM, T. & NORMAN, B. 1983 Some basic aspects of the wet pressing of paper. *J. Pulp Paper Sci.* **84a,** TR101–106.

CHANG, N. L. 1978 Dynamic compression of handsheets. In *TAPPI Engineering Conference Proceedings*, Book 1, pp. 93–106.

CECKLER, W. H. & THOMPSON, E. V. 1982 Final report of the University of Maine at Orono Wet Pressing Project. Report DOE/CS/40064-3 (DE83009342).

ERINGEN, C. A. 1976 (Ed.), *Continuum Physics*, Vol. III. Academic Press, New York.

FLÜGGE, W. 1972 *Tensor Analysis and Continuum Mechanics*, Springer-Verlag, Berlin.

GREEN, A. E. & NAGHDI, P. M. 1965 A dynamical theory of interacting continua. *Int. J. Engng Sci.* **3,** 231–241.

GREEN, A. E. & NAGHDI, P. M. 1970 The flow of fluid through an elastic solid. *Acta Mech.* **9,** 329–340.

JEWETT, K. B. 1980 Master's Thesis, Univ. of Maine at Orono, ME.

KUBIK, J. 1986 On internal coupling in dynamic equations of fluid-saturated porous solid. *Int. J. Engng Sci.* **24,** 981–989.

LODGE, A. S. 1974 *Body Tensor Fields in Continuum Mechanics*. Academic Press, New York.

MACGREGOR, M. A. 1985 What happens during shell and groove marking. *TAPPI Jl* **68,** 84–91.

NILSSON, P. & LARSSON, K. O. 1964 Paper web performance in a press nip. *Pulp Paper Mag. Canada* **69,** 66–73.

ROUX, J. C. 1986 Modélisation et optimisation du fonctionnement d'une section de presse(s) Thèse de Doctorat, Ecole Francaise de Papeterie.

ROUX, J. C. & VINCENT, J. P. 1985 Mathematical model of a press section. *Rev. Assoc. Techn. Ind. Papier* **39,** 543–550.

SINGH, K. M. 1990 Analysis of the wet pressing of paper pulp. Ph.D. Dissertation, State Univ. of New York, NY.

SWAIN, G. E. 1980 Behavior of press felts in compression. In *TAPPI Engineering Conference Proceedings*, Book 1, pp. 53–61.

THIGPEN, L. & BERRYMAN, J. G. 1985 Mechanics of porous elastic materials containing multiphase fluid. *Int. J. Engng Sci.* **23,** 1203–1214.

WAHLSTROM, P. B. 1960 A long term study of water removal and moisture distribution on a newsprint machine press section, Part I. *Pulp Paper Mag. Canada* **61,** T379–401.

WILDER, J. E. 1967 The fluid mechanics of plain press nips. *TAPPI Jl* **50,** 180–186.

YIH, C. S. & MCNAMARA, S. J. M. 1964 An initial study of the water removal process in the plain press nip, Part I. *TAPPI Jl* **47,** 153–156.

APPENDIX A

Constitutive Equation for a Viscoelastic Fiber Mat

The case of a viscoelastic solid is easily derived by combining the elastic and viscous properties. Let us write

$$T^{ij}\left(\gamma_{ij}, \frac{\mathrm{d}g_{ij}}{\mathrm{d}t}\right), \tag{A1}$$

where the rate of change in the metric (rate of strain) is computed along a particle trajectory. Since we consider a steady-state flow in the x^1 direction, we have

$$\frac{\mathrm{d}g_{ij}}{\mathrm{d}t} = u^1 \frac{\partial g_{ij}}{\partial x^1}. \tag{A2}$$

Consequently, the stress tensor can be expressed as

$$T^{ij} = \frac{E^{ijkm}\gamma_{km}}{2} + F^{ijkm}u^1 \frac{\partial g_{km}}{\partial x^1}. \tag{A3}$$

The elastic terms are calculated as above; the viscous term can be expressed in terms of the Christoffel symbols, as

$$F^{ijkm}u^1 \frac{\partial g_{ij}}{\partial x^1} = F^{ijkm}u^1(g_{mn}\Gamma^n_{k1} + g_{nk}\Gamma^n_{m1}). \tag{A4}$$

If the viscous part of the stress is expressed in terms of the velocity derivatives, we have

$$S^{ij} = \frac{1}{2}\left(g^{jk}\frac{\mathrm{D}u^i}{\mathrm{D}x^k} + g^{ik}\frac{\mathrm{D}u^j}{\mathrm{D}x^k}\right). \tag{A5}$$

When the partial derivatives of the velocity vanish (see the next appendix), the expression reduces to

$$S^{ij} = \tfrac{1}{2}(g^{jk}\Gamma^i_{km}u^m + g^{ik}\Gamma^j_{km}u^m). \tag{A6}$$

Under a "Newtonian" assumption, the viscous part of stress is then

$$T^{ij} = 2\mu_s S^{ij} = \mu_s(g^{jk}\Gamma^i_{km}u^m + g^{ik}\Gamma^j_{km}u^m). \tag{A7}$$

Comparison of [20] and [23] shows that consistency is achieved with the phenomenological coefficients F:

$$F^{ijkm} = \mu_s g^{ik}g^{jm}. \tag{A8}$$

APPENDIX B

Equations in Terms of Primary and Secondary Variables

The introduction of secondary variables ([B7]–[B28]) yields [B1]–[B6].

Compatibility equation,

$$\epsilon_{11}|_{22} + \epsilon_{22}|_{11} + 2\epsilon_{12}|_{12} = 0. \tag{B1}$$

Total material momentum balance, in the x^1 direction,

$$v_{27} = \frac{\mathrm{D}T^{11}}{\mathrm{D}x^1} + \frac{\mathrm{D}T^{12}}{\mathrm{D}x^2}. \tag{B2}$$

Total material momentum balance, in the x^2 direction,

$$v_{28} = \frac{\mathrm{D}T^{12}}{\mathrm{D}x^1} + \frac{\mathrm{D}T^{22}}{\mathrm{D}x^2}. \tag{B3}$$

Water momentum balance, in the x^1 direction,

$$v^{23} = \alpha U^1 + \frac{\mathrm{D}(prg^{11})}{\mathrm{D}x^1} + \frac{\mathrm{D}(prg^{12})}{\mathrm{D}x^2}. \tag{B4}$$

Water momentum balance, in the x^2 direction,

$$v_{24} = \alpha U^2 + \frac{\mathrm{D}(prg^{12})}{\mathrm{D}x^1} + \frac{\mathrm{D}(prg^{12})}{\mathrm{D}x^2}. \tag{B5}$$

Water mass balance,

$$p_{\mathrm{w}} \frac{\mathrm{D}U^1}{\mathrm{D}x^1} + p_{\mathrm{w}} \frac{\mathrm{D}U^2}{\mathrm{D}x^2} + U^1 \frac{\mathrm{d}p_{\mathrm{w}}}{\mathrm{d}x^1} + U^2 \frac{\mathrm{d}p_{\mathrm{w}}}{\mathrm{d}x^2}. \tag{B6}$$

Stress–strain relations,

$$T^{11} = \frac{E}{2(1+\nu)}\left[\frac{2\nu}{1-2\nu} g^{11} g^{km} + 2g^{lk} g^{lm}\right][g_{km} - g^0_{km}], \tag{B7}$$

$$T^{12} = \frac{E}{2(1+\nu)}\left[\frac{2\nu}{1-2\nu} g^{12} g^{km} + 2g^{1k} g^{2m}\right][g_{km} - g^0_{km}] \tag{B8}$$

and

$$T^{22} = \frac{E}{2(1+\nu)}\left[\frac{2\nu}{1-2\nu} g^{22} g^{km} + 2g^{2k} g^{2m}\right][g_{km} - g^0_{km}]. \tag{B9}$$

Secondary variable definitions

Determinant of the metric tensor,

$$g = g_{11} g_{22} - g_{12}^2. \tag{B10}$$

Contravariant metric tensor components,

$$g^{11} = \frac{g_{22}}{g}, \tag{B11}$$

$$g^{12} = \frac{-g_{12}}{g} \tag{B12}$$

and

$$g^{22} = \frac{g_{11}}{g}. \tag{B13}$$

Strain tensor components,

$$\epsilon_{11} = g_{11} - g^0_{11} \quad [B14]$$

$$\epsilon_{12} = g_{12} - g^0_{12} \quad [B15]$$

and

$$\epsilon_{22} = g_{22} - g^0_{22}. \quad [B16]$$

Water fraction in the material,

$$\phi = \frac{g - (1 - \phi_0)g_0}{(1 - \phi_0)g_0}. \quad [B17]$$

Partial density of the water phase,

$$p_w = \phi \text{ (water density)}. \quad [B18]$$

Partial density of the solid phase,

$$p_s = \phi + (\text{solid-phase density})(1 - \phi_0)g_0. \quad [B19]$$

Definition of the initial metric tensor components,

$$g^0_{11} = \left(\frac{a^2(11 - g_{11})^2 + V^2 g^2_{22}}{(11 - g_{11})^2 + g^2_{12}}\right), \quad [B20]$$

$$g^0_{12} = \left(\frac{V^2 - a^1(11 - g_{11})}{(11 - g_{11})^2 + g^2_{12}}\right) \quad [B21]$$

and

$$g^0_{22} = \left(\frac{a^2(11 - g_{11})^2 + a^2 g^2_{22}}{(11 - g_{11})^2 + g^2_{12}}\right). \quad [B22]$$

Definition of variable 23,

$$v_{23} = p_w\left(U^1 \frac{DU^1}{Dx^1} + U^2 \frac{DU^1}{Dx^2}\right). \quad [B23]$$

Definition of variable 24,

$$v_{24} = p_w\left(U^1 \frac{DU^2}{Dx^1} + U^2 \frac{DU^2}{Dx^2}\right). \quad [B24]$$

Total material velocity in direction c^1,

$$u^1 = \frac{(p_w U^1 + (p_s - p_w)V)}{p_s}. \quad [B25]$$

Total material velocity in direction x^2,

$$u^2 = \frac{(p_w U^2 + (p_s - p_w)0)}{p_s}. \quad [B26]$$

Definition of variable 27,

$$v_{23} = p_s\left(u^1 \frac{Du^1}{Dx^1} + u^2 \frac{Du^1}{Dx^2}\right). \quad [B27]$$

Definition of variable 28,

$$v_{27} = p_s\left(u^1 \frac{Du^2}{Dx^1} + u^2 \frac{Du^2}{Dx^2}\right). \quad [B28]$$